Photothermal convection of a magnetic nanofluid in a direct absorption solar collector

Boris V. Balakin [a,*], Mattias Stava [b], Anna Kosinska [a]

[a] *Western Norway University of Applied Sciences, Bergen, Norway*
[b] *University of Bergen, Department of Physics and Technology, Bergen, Norway*

ARTICLE INFO

ABSTRACT

Nanofluid-based direct absorption of solar heat results in thermal efficiencies superior to conventional solar thermal technology. In addition, convection of nanofluid can be sustained pump-free in the collector. In this article, we study an aqueous magnetic nanofluid capable to establish the *photothermal* convection in a lab-scale direct absorption solar collector equipped with a solenoid. The nanofluid consisted of 60-nm Fe_2O_3 particles dispersed in distilled water at concentration in the range 0.5% wt.-2.0% wt. An empirical model of the *photothermal* convection was developed based on the experiments. The model accounted for magnetic and thermophoretic forces acting within the nanofluid. The nanofluid with up to 2.0% wt. iron oxide nanoparticles obtained the velocity of ~5 mm/s under the magnetic field of up to 28 mT. This resulted in the maximum thermal efficiency of the collector equal to 65%.

1. Introduction

Nanofluids were developed by Choi and Eastman (1995) to increase the thermal conductivity of the existing heat transfer fluids and then to boost the coefficient of heat transfer during forced convection. However, the use of nanofluids for forced convection has inherent drawbacks (Rudyak and Minakov, 2018). The presence of nanoparticles increases the apparent viscosity of the nanofluids so that the pumping cost grows. Another issue connected to the use of the concentrated nanofluids is their possible nanotoxicity (Bostan et al., 2016) and erosion.

These limitations hinder the replacement of the conventional heat transfer fluids by nanofluids. Although Hydromx (2021) reports various applications of their commercial nanofluids for domestic hot water and data centres, the scientific community considers the industrial use of the nanofluids as limited due to the discussed challenges.

An alternative thermal application of nanofluids allows for much lower amounts of nanoparticles. The diluted nanofluids are used in direct absorption solar collectors (DASC) (Viskanta, 1987; Gorji and Ranjbar, 2016). In this case, the nanofluid acts both as a receiver of solar radiation and a heat transfer fluid. By collecting the radiated heat in the bulk of the fluid, the nanofluids reduce the average surface temperature of the collector and thus limit the collector's thermal loss to the environment. Starting from miniature DASCs (Alberghini et al., 2019; Otanicar et al., 2010), the nanofluid-based solar thermal technology has advanced towards laboratory scale prototypes (Gupta et al., 2015).

Karami et al. (2015) tested a flat DASC prototype based on the water–glycol nanofluid with CuO nanoparticles with a concentration of 1.5 wt%. The maximum thermal efficiency of the collector was 65%. A similar efficiency of 60% was measured by Singh and Khullar (2020) for a concentrating DASC with a paraffin-based nanofluid laden with a 1.0 vol.% of soot particles. Karami's DASC with a carbon-based nanofluid (1.3% wt.) was also tested by Delfani et al. (2016). In this case, the efficiency increased to 90%, which was 45% over the efficiency of an equivalent flat-plat collector with an opaque black surface.

Vakili et al. (2016) documented a thermal efficiency of 90% for a prototype DASC with a 0.005% wt. nanofluid. The best photothermal conversion was obtained by Kumar et al. (2020) who found that a 0.0002% wt. of gold nanoparticles brought the maximum thermal efficiency of DASC up to 95%. Most recently, Moravej et al. (2021) presented a hemispherical design of DASC filled by an aqueous nanofluid consisting of 0.3% silver nanoparticles. Despite the collector's interesting design, the maximum efficiency of 61% was lower than that of the majority of other prototype DASCs.

The aforementioned maximum thermal efficiencies of direct absorption solar collectors are higher than the efficiency provided for most commercial flat-plate solar collectors. However, the superiority of the existing prototype DASCs diminishes at higher operating temperatures

---

due to enhanced thermal leaks. In this condition, the efficiency of DASCs is between 20% and 40% lower than the efficiency of a commercial solar collector (Goel et al., 2020). Hence, additional studies on better thermal insulation of the prototypes are required. However, the thermal insulation of DASCs is a rather challenging problem, as the size and volume of the nanofluid layer present in a DASC are larger than the thin metal receivers used in conventional solar collectors.

Another method to boost the performance of DASCs is to increase the system's total efficiency, reducing the pumping costs via the establishment of natural convection in the collector's flow loop. There exist domestic hot water systems where the elevation difference in the flow loop drives natural convection. This opens up an opportunity for a pump-free operation of the loop, which also reduces the system's capital costs.

However, the architecture of modern buildings demands that the renewable energy systems fit the building's profile. Such requirements limit the elevations and alter the tilt angles of solar collectors suppressing the natural convection. To address the challenge, Jin et al. (2020, 2019) developed a direct absorption oscillating heat pipe with transparent walls. The heat pipe was filled with aqueous nanofluids with 18 nm gold nanoparticles (0.024 wt%) and carbon nanotubes (3 wt%) of micrometric length. Under natural solar conditions, the photothermal boiling (Ulset et al., 2018) propelled the nanofluid through the heat pipe. Although an excellent thermal efficiency of 92% was detected for the case with carbon nanotubes, the entire concept does not seem feasible from the practical point of view due to the need for vacuumisation of the pipe and challenges associated with the long-term stability of the micrometric particles.

The pump-free operation of DASCs becomes possible without natural convection, appealing to the second feature of the metal-based nanofluids, namely the *magnetic convection*. When the nanofluid is simultaneously subjected to a temperature gradient and a magnetic field, a magnetic Kelvin force pumps the nanoparticles due to the difference between the magnetic moments of the colder and the warmer particles (Aursand et al., 2016b). To our knowledge, there are no research papers on DASCs with pure magnetic convection of nanofluid, even though several works consider the influence of the magnetic field on the performance of DASCs with the forced convection of ferrofluids.

He et al. (2016) considered how a radial magnetic field of 3 mT influences the efficiency of a lab-scale DASC with an aqueous nanofluid with 30 nm Co nanoparticles. In their research, the nanofluid flows through the collector via an ordinary pump. Most possibly, the magnetic field was supposed to boost the performance establishing a secondary convective flow of the nanofluid in the radial direction and thus enhancing the mixing. According to the collector's grade curve, the maximum thermal efficiency of a magnetised nanofluid was around 85%, which was 13% higher than for cases with no magnetic field applied.

Two interesting papers by Alsaady et al. (2019) and Liu et al. (2018) were dedicated to the experiments on a DASC with magnetic nanofluid and solar concentration (∼×16). The magnetic nanofluid was based on 10 nm magnetite particles dispersed in water. As in the experiments by He et al. (2016), a water pump established the flow of the nanofluid while the magnetic field of 3–11 mT was set in the axial direction. The maximum thermal efficiency of 41% was measured for the DASC subjected to 10.47 mT. This efficiency was about 25% higher than for the nanofluid-based DASC without any magnetic field. These papers did not entirely clarify what the physical reason for the notable rise of photothermal performance was, namely a magnetic-driven mixing enhancement or an additional pumping pressure difference. None of the papers on magnetic pumping in DASC considered the influence of thermophoresis on the thermal performance of collectors.

In our experimental work shown in this paper, we prove a concept of a pump-free operation of DASC with a magnetic nanofluid. The combination of an external magnetic field and thermophoresis with a photothermal absorption of radiate heat makes it possible to establish continuous *photothermal convection* in the collector. We consider how the nanoparticles' concentration and the magnetic field's strength influence the thermal performance of a closed photothermal flow loop.
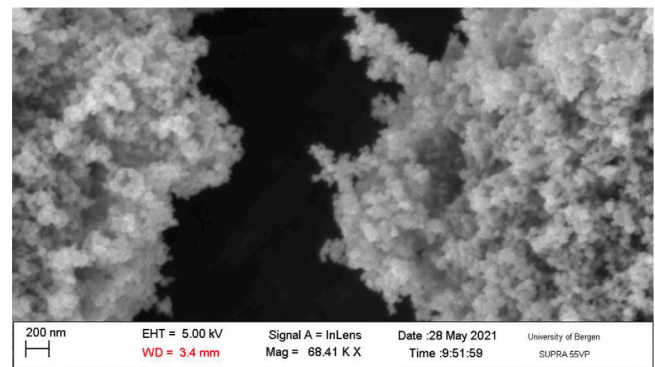

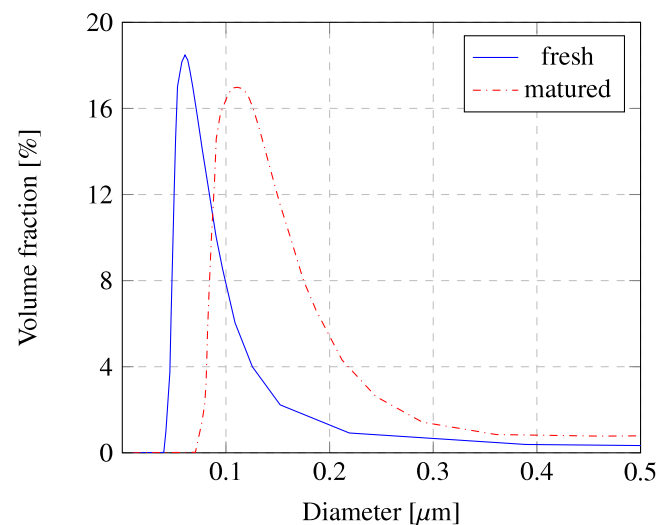**Fig. 1.** Scanning electron microscopy images of iron oxide particles.

Fig. 2. Particle size distribution in 1.0 wt% nanofluid for freshly prepared and matured samples.

2. Methodology

The experiments on photothermal convection were carried out at a laboratory scale in a tubular rig containing a direct absorption solar collector with a magnetic nanofluid.

2.1. Nanofluid

The nanofluid was produced by dispersing nanoparticles of iron oxide (Fe_2O_3) in water. The nanoparticles were purchased from Sigma Aldrich. According to the manufacturer, the size of the particles, determined by the Brunauer–Emmett–Teller technique, was below 50 nm (Sigma Aldrich, 2021). The results of the scanning electron microscope Jeol JSM-7400F are shown in Fig. 1. The individual particles are at least 25% of the experimental scale, confirming the information from the manufacturer.

A two-step method was used to produce the nanofluid. In the first step, the required mass of the nanoparticles was mixed with a corresponding volume of distilled water (Fybikon, Norway). The fraction of particles was measured using the precision scale Sartorius CPA 324S (±0.1 mg). The mixture was mechanically stirred to form a suspension.

In the second step, the suspension was subjected to intense sonication for 30 min. The ultrasonic treatment of the suspension was conducted using the ultrasonic bath Branson 3510 at 130 W. To avoid possible electromagnetic and rheological influence of surfactants on the
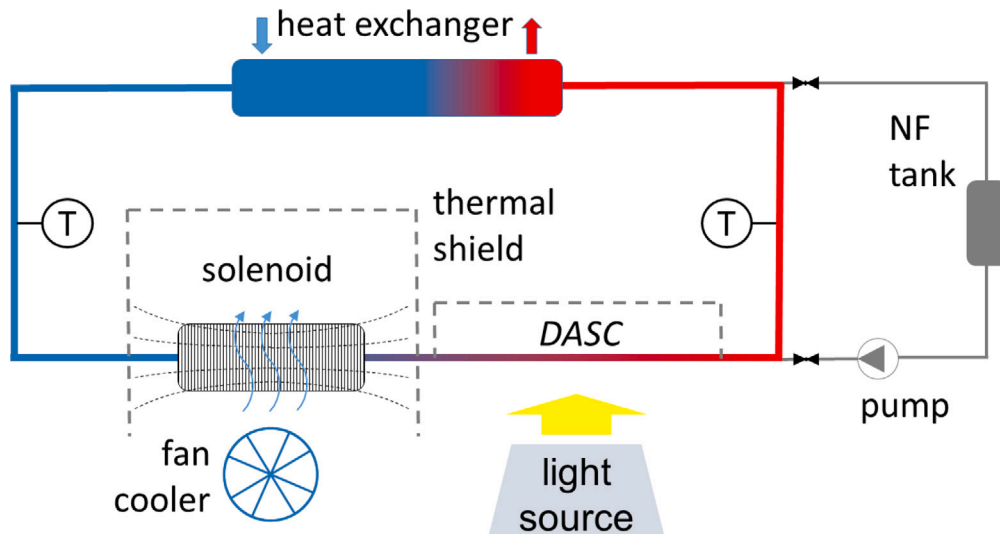
Fig. 3. A schematic of the experimental set-up.

studied photothermal convection, the obtained nanofluid was produced without an electrochemical stabilisation. The freshly made batches of the nanofluid were used in the experiments within 24 h after production without further treatment. The nanofluid remained visually stable during this period.

The distribution of particle sizes in the nanofluid was inspected by means of static light scattering (SLS) using Malvern Mastersizer 2000. The particle size distribution for the freshly produced sample is presented in Fig. 2. From the figure, we note that the agglomeration of the nanoparticles in the fresh nanofluid resulted in an average particles size of 60 nm. The size distribution for the samples treated in the experiments is also presented in Fig. 2. The combined heating and magnetisation increased the average particle size to 110 nm. According to the literature, nanoparticles with sizes of about 100 nm remain stable after an ultrasonic dispersion in water (Moldoveanu et al., 2018). Therefore, we conclude on partial stability of the matured samples.

2.2. Experimental system

As shown schematically in Fig. 3, the experimental system consisted of a flow loop, a direct absorption solar collector, a heat exchanger, and a solenoid. The flow loop was made of polytetrafluoroethylene tubes with an internal diameter of 4 mm and a wall thickness of 2 mm. The length of the sections for temperature measurement was 200 mm, the length of the section with the heat exchanger was 400 mm, and the length of the heat exchanger was 100 mm. The temperature was measured in 200 mm sections using the T-type thermocouples ($\pm$0.3 K) connected to HH506RA Multilogger from Omega. The direct absorption solar collector was a part of a 400 mm long transparent glass tube with an internal diameter of 4 mm.

The flow loop was connected to a 50 ml cylindrical expansion tank open to the atmosphere. The tank was a part of a replenishing line used during the filling and draining of the flow loop. A microdiaphragm pump circulated the nanofluid through the line at 5 l/min. This injection line was inactive during the experiments.

The heat exchanger was of a shell-and-tube type. The internal tube of the heat exchanger was a glass spiral with nine rounds and major diameter of 20 mm. The inner diameter of the tube in the spiral was 4 mm. The inner diameter of the shell was 31 mm, and the wall thickness was 2 mm. The heat exchanger was cooled down by tap water at 12 °C.

The glass tube consisted of the solenoid region and the DASC region. The DASC region was a 100 mm long part of the tube that was placed under the external radiation. The radiation was directed from a halogen

lamp OSRAM (Haloline 230 V, 400 W). The spectrum of the lamp was shifted by 350 nm to the red zone if compared to the solar spectrum (Ulset et al., 2018). The amount of radiated heat meeting the DASC surface was 2.8 W. This value was measured using an LS122 IR radiometer from Linshang.

The solenoid (FC-5818 from APW) was mounted over the glass tube. The length of the magnetic coil was $l = 44.7$ mm with, the outer and inner diameters of the bobbin being 38.1 and 19.1 mm, respectively. The coil consisted of $n = 800$ turns with the total resistance of 5.75 Ω. The solenoid operated under 6 V, altering the current I from 0 to 1.26 A using a DC power supply. The maximum of the magnetic field $H^{\max} \sim In/l$ in the solenoid was varied between 0 and 28.2 mT. The current and voltage were controlled by a UT131B multimeter from UNI-T. The coil was coupled with a 7.2 W processor cooler from Foxconn to remove the Joule heat from the solenoid. A thermally-insulating shield covered the solenoid and the cooler to protect the DASC from the cooling by the fan.

The experimental rig operated as follows. At first, the nanofluid was injected into the loop using the pump. After flashing the lines during the continuous operation of the pump, the injection line was closed. The lamp was then activated, and the electrical current was set in the coil. The multilogger recorded the temperature for about 1 h until the measurement arrived at a steady state. The experiments were run at an ambient temperature of 21.3 $\pm$ 1.2 °C. Next, the nanofluid was drained from the flow loop, the system was dismantled, and the pipes were cleaned internally by pigging. The last stage included cleaning the tubes in the ultrasound bath filled with ethanol.

2.3. Mathematical model

It is interesting to obtain an estimate of the flow rate induced in the rig due to the photothermal convection. However, direct measurement of small-magnitude convective currents is challenging as the nanofluid is simultaneously subjected to thermal and magnetic radiation, which influences measurements. Therefore, we arranged for a theoretical calculation.

First, we state that convection is possible when the mechanical energy of particulate motion increases enough to balance the frictional flow resistance in the loop. For this model, we assume that the most significant contribution to the nanoparticle motion is due to thermophoresis and magnetic field. In terms of the pressure drop, this means that the positive pressure differences induced in the solenoid Δp_m and thermophoresis Δp_T are balanced by the frictional pressure drop Δp_f established in the loop at a given mean flow velocity of convection
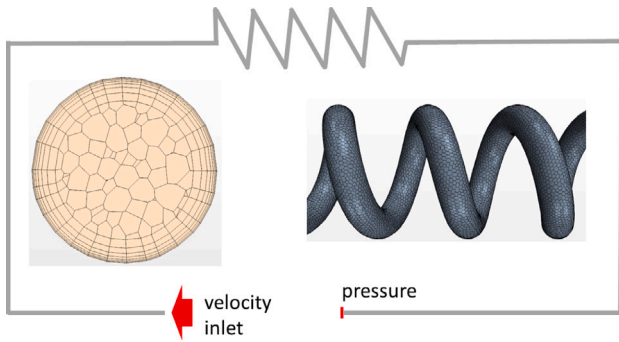
Fig. 4. The computational mesh and geometry used in the computational fluid dynamics simulations.

v. The contribution of the magnetic field is estimated from Aursand et al. (2016b,a):

$$\Delta p_m \sim \phi_p \mu_0 M_m H^{\max}, \tag{1}$$

where ϕ_p is the volume fraction of the nanoparticles, μ_0 is the vacuum permeability.

Also, M is the magnetisation of the particles (Aursand et al., 2016a):

$$M_m = M^s \mathcal{L} \left(\frac{\mu_0 V_p M^s H^{\max}}{k_B T} \right), \tag{2}$$

where $\mathcal{L}$ is the *Langevin* function (Aursand et al., 2016b), V_p is the volume of a particle, T is the temperature of the nanofluid, and k_B is the Boltzmann constant. The saturation magnetisation M^s is given as Aursand et al. (2016a):

$$M^s = M^* \left(1 - \frac{T - T_r}{T_c - T_r} \right), \tag{3}$$

where $M^* = 35.9$ kA/m is the saturation magnetisation of Fe_2O_3 at the reference temperature $T_r = 300$ K (Lassoued et al., 2018), and $T_c = 960$ K is the Curie temperature (Muench et al., 1981).

The thermophoretic pressure drop is given after Brock (1962):

$$\Delta p_T = \frac{-6n_p \pi \mu_l v_l d C_s}{1 + 6C_m Kn} \frac{k_l/k_p + 2C_t Kn}{1 + 2k_l/k_p + 4C_t Kn} \frac{\Delta T}{T}, \tag{4}$$

where ΔT is the temperature difference in the loop, k is the thermal conductivity of the base fluid (l) and the particles (p), d is the average particle size, n_p is the number density of the particles, μ and v are the dynamic and the kinematic viscosity, Kn is the Knudsen number of the particles, and coefficients $C_s = 1.17$, $C_t = 2.18$ and $C_m = 1.14$ (Crowe et al., 1998).

We determined the mean flow velocity from a steady force balance:

$$\Delta p_m + \Delta p_T = \Delta p_f, \tag{5}$$

where the pressure drop due to the friction of the nanofluid was computed following Idelchik (1986):

$$\Delta p_f = \xi \rho \frac{v^2}{2}, \tag{6}$$

where ξ is the dimensionless total flow resistance of the system. We developed a single-phase supplementary computational fluid dynamics (CFD) model to define the flow resistance.

The simulated geometry, shown schematically in Fig. 4, represented the pipes from the experimental rig excluding the solenoid section. The computational domain was discretised using 0.5 mm polyhedral control volumes. The control volumes were adjusted to a near-wall subsurface by seven layers with prismatic cells (Fig. 4). We optimised the mesh by running a mesh dependence study.

As presented in the figure, the boundary conditions included the velocity inlet and the pressure outlet. The Reynolds number was less
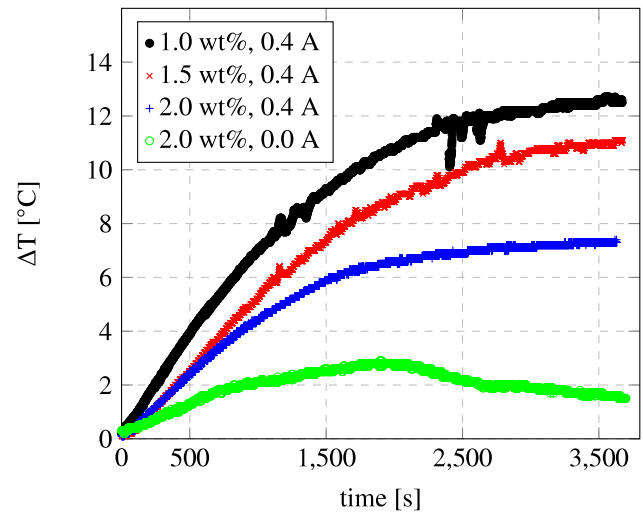

Fig. 5. Temperature difference vs. time for different values of the particle concentration and magnetic field.

than 1000 in all the simulations. A steady laminar flow of incompressible fluid was modelled using a single system of Navier–Stokes equations (Anderson, 1995). The numerical solution was carried out in a commercial package STAR-CCM+ from Siemens (v.13.06.012). The CFD model did not account for thermophoresis and magnetic effects. The Navier–Stokes equations were discretised in space through the second-order upwind scheme. The flow was solved using SIMPLE with the following under-relaxation coefficients: velocity 0.3, pressure 0.1. The solution converged at the residuals below 10^{-6}.

3. Results and discussion

3.1. Temperature difference

The first experiments were conducted to clarify how the concentration of nanoparticles influences the photothermal heating in the system. For this purpose, we recorded the temperature difference in the loop without magnetic field at different concentrations of nanoparticles and at 0.4 A in the solenoid. This is shown in Fig. 5 as dynamic temperature curves. From the plot, we note that the temperature differences increase in time and reach a steady value after approximately 2500 s of the process. The maximum difference of 12.4 °C is seen for the concentration of 1.0% wt. The average combined experimental uncertainty of the data from the figure was 0.6 K. By increasing the concentration, the temperature difference decreased to 7.8 °C at 2.0% wt. We also note that the thermal stabilisation of the system occurs faster for higher concentrations. We return to this issue later in the paper, where we introduce the notion of the characteristic time of thermal stabilisation.

We observed a continuous flow of nanofluid during the measurements in the DASC and heat exchanger. The flow started after the solenoid was activated and was thus induced by the magnetic convection due to the formation of temperature gradients in the rig. An increase in the flow rate can explain the reduction of the temperature difference for higher particle concentrations. The increase was obviously dependent on the number of magnetic particles as they drove the fluid via the interphase momentum coupling.

Several mechanisms are responsible for the observed reduction of the temperature. At first, by enhancing the flow rate, we limited the radiant heat exposure to the particles. Next, increased flow enhances the heat transfer in the heat exchanger and increases the thermal leaks to the environment. In addition, increasing the concentration of the nanoparticles, we increased the thermal conductivity of the nanofluid (Colla et al., 2012) and further promoted heat exchange
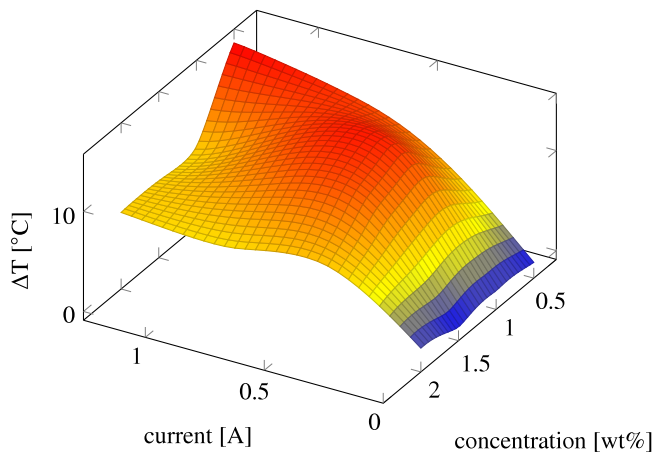
Fig. 6. Temperature difference for different concentrations and electric currents.

Fig. 7. Loop flow resistance for different Reynolds numbers.

Fig. 8. Computed flow velocity as a function of electric current for different concentrations of particles.

with the cold environments. Similar qualitative behaviour of heating in a conventional direct absorption solar collector was reported in the recent work by Struchalin et al. (2021).

To verify whether natural convection occurs in the rig, we irradiated the DASC section of the loop for about an hour without activating the solenoid. A dynamic temperature log for 2.0% wt. nanofluid in the absence of a magnetic field is presented in Fig. 5 as a reference. According to the temperature logs, the steady-state temperature difference was 0.9 ± 0.4 °C when using various nanoparticle concentrations. This low value of the temperature difference was due to a very slow fluid circulation in the loop, which was also confirmed visually in the transparent sections of the pipes.

In the next series of experiments, we tested how the magnetic field and concentration simultaneously influenced the process. Fig. 6 shows a 3D-surface representing the temperature difference as a function of electrical current in the solenoid and the mass fraction of nanoparticles. The surface was obtained by connecting the array of experimental points by splines.

In general, according to the figure, the temperature difference reduces with the current and particle concentration increase. Nevertheless, this happens after the optimal values of concentration (about 1.0% wt.) and current (∼0.7 A) are reached. At the maximum current, the temperature difference increased for the lowest concentrations. This indicates that the maximum flow was established for each studied concentration at 1.26 A that corresponded to a magnetic field of 28 mT. This value was 2.5 times greater than the field used in Alsaady et al. (2019) and Liu et al. (2018).

There was very low velocity for moderate currents at concentrations below 1.0% wt. As discussed above, the momentum of particles was not sufficient to drive the flow in this case. Another possible reason for the maximising of the temperature gradient at this concentration could be a maximisation of photothermal performance in the DASC.

3.2. Flow velocity

As previously mentioned, we determined the total flow resistance using CFD simulations. Fig. 7 shows the results by demonstrating how the Reynolds number influences this parameter. To calculate the latter, we followed Buschmann et al. (2018) who found that the equivalent thermophysical properties may be used to determine dimensionless criteria for stable nanofluids. The density of the nanofluid was computed as $\rho_{nf} = \rho_l(1 - \phi_p) + \rho_p \phi_p$, where ρ is the density of the base fluid (l) and the particles (p). We determined the apparent dynamic viscosity of the nanofluid according to Colla et al. (2012):

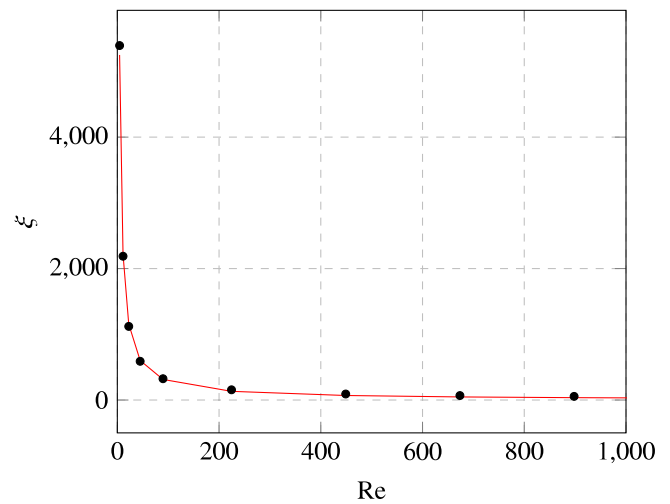$$\mu_{nf} = \mu_l (1 - \alpha \phi_p - \beta)^{-2}, \tag{7}$$
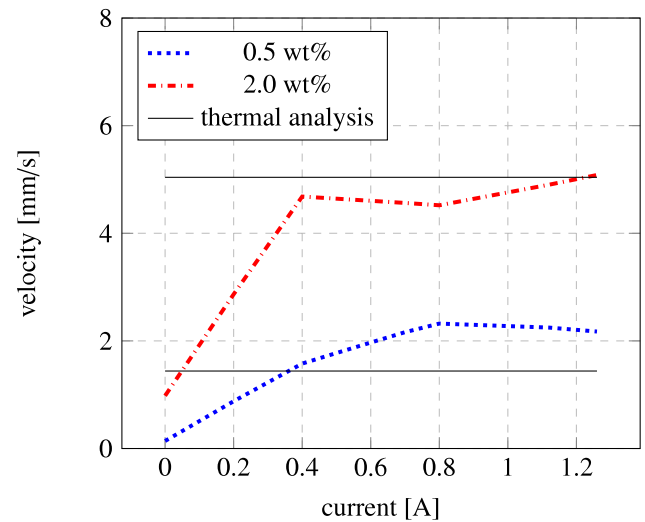
where $\alpha = 0.073$ and $\beta = 0.034$ are the empirical coefficients.

The total flow resistance reduces from $\xi = 5249$ at Re $= 4.5$ to $\xi = 55.4$ at Re $= 899$. We fitted the dependence using a power-law function: $\xi = 21573 \text{Re}^{-0.94}$ with $R^2 = 0.99$. This is shown in Fig. 7.

Fig. 8 presents the mean flow velocity estimated using Eq. (5). We note from the figure that the mean flow velocity is below 1 mm/s for the cases without magnetic field. Thermophoresis was the only source of momentum capable of driving the flow. In these cases, the computed flow velocity increased with the particle concentration from 0.14 mm/s at 0.5% wt up to 0.98 mm/s at 2.0% wt.

By applying the magnetic field, we increased the mean flow velocity several times. The steady mean flow velocity was about 2 mm/s for 0.5% wt. and 5 mm/s at 2.0%wt. We note that the flow velocity did not increase significantly when altering the current above 0.5 A. In this case, thermophoresis became the main driving force of the motion in the system. An average magnetic pressure drop Δp_m was $14.0 \pm 6.7\%$ of the thermophoretic Δp_T. However, the thermophoretic motion of the nanofluid is possible when a temperature difference is established in the loop. The temperature difference is triggered by the magnetic pressure, which was under 9% of the thermophoretic pressure at low currents.

A further enhancement of the magnetic field increased the magnitude of the flow and flattened the temperature difference. This decreased the thermophoretic pressure, so the flow rate reached an equilibrium. At the maximum current, the pressure drop caused by the magnetic field increases to 28% of the thermophoretic pressure drop. The system self-limits the flow velocity under the variable magnetic current.

3.3. Thermal analysis

To verify the calculation of the mean flow velocity, we conducted a thermal analysis of the system. At first, from the dynamic temperature curves (see Fig. 5), we extracted the thermal response time of the system τ_T. This characteristic time is defined as a temporal interval between the start of the process and the moment when the temperature difference becomes 63.2% of the steady-state value (Lewis et al., 2004). Nevertheless, due to the spread of experimental data, there was an uncertainty in the determination of the steady-state condition. Therefore, in the calculations, we used an average thermal response time $\tau_T = 37.3 \pm 9.3$ min. This value resulted from the entire set of experiments with the magnetic field.

Next, assuming the most intensive heat transfer took place in the heat exchanger, we calculated the heat transfer coefficient there as Lewis et al. (2004):

$$\alpha_s = \frac{\rho_{nf} V C_{nf}}{\tau_T A_s},\tag{8}$$

where α_c is the heat transfer coefficient in the heat exchanger, V is the total volume of the nanofluid, $C_{nf} = C_l(1-\phi_p)+C_p\phi_p$ is the specific heat of the nanofluid, and A_s is the area of the spiral in the heat exchanger. An average coefficient of the heat transfer in the exchanger became 5.7 ± 1.5 W/m^{2}K.

Balancing the heat in the system, we computed the volume flow of the nanofluid, and the mean flow velocity:

$$\rho_{nf} Q C_{nf} \Delta T = G - \alpha_a(\overline{T} - T_a)A_t + \epsilon\sigma(\overline{T}^4 - T_a^4)A_t + \alpha_s(\overline{T} - T_c)A_s,\tag{9}$$

where ΔT is the temperature difference in the loop, Q is the volume flow of the nanofluid, G is the incident thermal radiation, $\overline{T}$ is the average temperature of the nanofluid, σ is the Stefan–Boltzmann constant, ϵ is the emissivity, A_t is the total area of the tubes (excluding the heat exchanger), and indices D, a, s denote DASC, ambient and heat exchanger conditions. We computed the coefficient of heat transfer between the tubes and the environment α_a using expressions for natural convection around a heated plate (Struchalin et al., 2021). The parameters in Eqs. (8)–(9) were calculated using the temperatures and the dimensions measured from the experiments.

The results of the thermal analysis (Eqs. (8)–(9)) are collected in Fig. 8 in the form of a band that contains 95% of the data, deviating around an average. According to the figure, a major part of theoretical prediction complies with the experiment-based thermal analysis. We also note that the nanofluid flow is only well established when the electric current was above 0.4 A and the particle concentration was 0.5% wt. For lower values of the current, the flow velocity may become discontinuous. This observation corresponds to Fig. 6.

3.4. Thermal efficiency

The thermal efficiency of the collector characterises the photothermal performance of the DASC. We calculated the efficiency according to the standard approach (Duffie and Beckman, 2013):

$$\eta = \frac{\rho_{nf} C_{nf} Q \Delta T}{G}.\tag{10}$$

The volume flow rate was computed using the mean flow velocity from the theoretical model (Eq. (6)). Fig. 9 illustrates how the thermal efficiency evolves with the current and concentration of particles. In
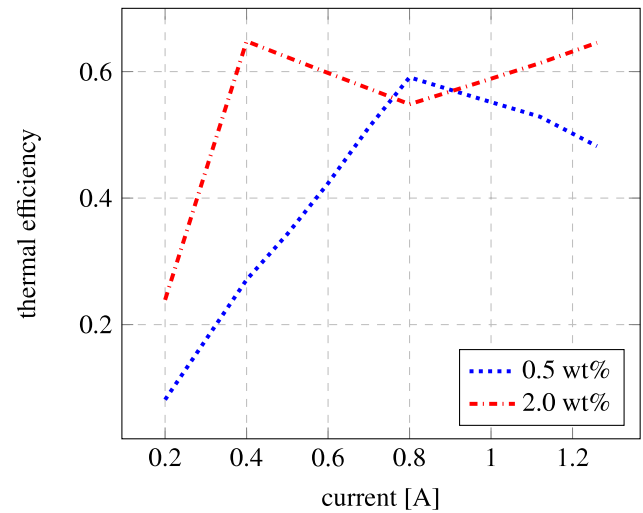

Fig. 9. Thermal efficiency as a function of electric current for different concentrations of particles.

general, the efficiency increases with the electric current. The thermal efficiency varies between 8% for the concentration of 0.5% wt. and the magnetic field of 8.9 mT and 65% for the concentration of 2.0% wt. and the magnetic field of 28.2 mT. When it comes to the concentration of particles, the efficiency at a concentration of 2% wt. is not less than at a concentration of 0.5% due to at least twice faster convection established in the loop. We note the *extremum* of 59% at a concentration of 0.5% wt. and electric current of 0.8 A. For this case, a better absorption of thermal radiation in DASC compensated for a deficient flow rate and so increased the efficiency.

For our system, the maximum value of the thermal efficiency is about 20% higher than those obtained by Alsaady et al. (2019) and Liu et al. (2018). Although our system demanded three-fold higher electromagnetic power and four-fold larger concentration, it was driven by approximately twice the lower solar heat flux. Therefore, considering Eq. (10), we conclude there is an equivalence of thermal performance between the systems.

We note that the described *photothermal* process is imperfect compared to the existing solar thermal systems with nanofluids. For instance, the efficiency of a DASC using pumps to circulate the fluid may come to 80% (Struchalin et al., 2021), which is significantly higher than in our experiments. In addition, when accounting for the consumption of electric power in our rig (up to 7.6 W), the system's total efficiency becomes negative. Therefore, the described process requires further improvement of nanomaterials with higher magnetic susceptibility and the more optimal design of the flow system. Nevertheless, even at the current stage, the technology can be used for the absorption and transfer of radiative heat in systems, which must exclude the mechanical actuation of flow (e.g., in biotechnology).

4. Conclusions

In this paper, we investigated the process of *photothermal convection* in a lab-scale direct absorption solar collector with magnetic nanofluid. The collector was mounted in a closed loop, which was cooled on the opposite side of the circuit. The continuous flow of the nanofluid was established under the simultaneous influence of the external source of radiative heat and the solenoid mounted on the tubes. The experiments revealed that the temperature drop between the cold and warm parts of the collector could rise to 14 K at the magnetic field of 28 mT and the nanoparticle concentration of 0.5% wt. According to our theoretical estimates, the maximum flow velocity for the established pump-free magnetic convection was 5.1 mm/s at 28 mT and the

concentration of 2.0% wt. The thermal efficiency of the collector was in the interval 8%–65% for the entire range of considered concentrations and solenoid currents. The maximum efficiency is comparable to the thermal efficiency of a commercial vacuum-tube collector operating in Northern climate conditions (Popsueva et al., 2021). Although the developed process finds promising applications in solar thermal technology, the current design requires good optimisation. Additional efforts are needed to reduce the consumed electrical power and, at the same time, limit the number of used nanoparticles as the concentrated nanofluids reduce the thermal efficiency of DASC and increase the pumping costs. An opportunity to boost the natural convection in a DASC establishing the supplementary *photothermal convection* should be considered in the future.

Declaration of competing interest

The authors declare that they have no known competing financial interests or personal relationships that could have appeared to influence the work reported in this paper.

Acknowledgements

References

Alberghini, M., Morciano, M., Bergamasco, L., Fasano, M., Lavagna, L., Humbert, G., Sani, E., Pavese, M., Chiavazzo, E., Asinari, P., 2019. Coffee-based colloids for direct solar absorption. Sci. Rep. 9 (1), 1–11.

Alsaady, M., Fu, R., Yan, Y., Liu, Z., Wu, S., Boukhanouf, R., 2019. An experimental investigation on the effect of ferrofluids on the efficiency of novel parabolic trough solar collector under laminar flow conditions. Heat Transf. Eng. 40 (9–10), 753–761.

Anderson, J.D., 1995. Computational Fluid Dynamics, the Basics with Applications. McGraw-Hill Education.

Aursand, E., Gjennestad, M.A., Lervåg, K.Y., Lund, H., 2016a. A multi-phase ferrofluid flow model with equation of state for thermomagnetic pumping and heat transfer. J. Magn. Magn. Mater. 402, 8–19.

Aursand, E., Gjennestad, M.A., Lervåg, K.Y., Lund, H., 2016b. Potential of enhancing a natural convection loop with a thermomagnetically pumped ferrofluid. J. Magn. Magn. Mater. 417, 148–159.

Bostan, H.B., Rezaee, R., Valokala, M.G., Tsarouhas, K., Golokhvast, K., Tsatsakis, A.M., Karimi, G., 2016. Cardiotoxicity of nano-particles. Life Sci. 165, 91–99.

Brock, J.R., 1962. On the theory of thermal forces acting on aerosol particles. J. Colloid Sci. 17, 768–780.

Buschmann, M.H., Azizian, R., Kempe, T., Juliá, J.E., Martínez-Cuenca, R., Sundén, B., Wu, Z., Seppälä, A., Ala-Nissila, T., 2018. Correct interpretation of nanofluid convective heat transfer. Int. J. Therm. Sci. 129, 504–531.

Choi, S.U.S., Eastman, J.A., 1995. Enhancing Thermal Conductivity of Fluids with Nanoparticles. Tech. rep, Argonne National Lab., IL (United States).

Colla, L., Fedele, L., Scattolini, M., Bobbo, S., 2012. Water-based Fe2O3 nanofluid characterization: Thermal conductivity and viscosity measurements and correlation. Adv. Mech. Eng. 4, 674947.

Crowe, C., Sommerfeld, M., Tsuji, Y., 1998. Multiphase Flow with Droplets and Particles. CRC Press.

Delfani, S., Karami, M., Akhavan-Behabadi, M.A., 2016. Performance characteristics of a residential-type direct absorption solar collector using MWCNT nanofluid. Renew. Energy 87 (1), 754–764.

Duffie, J.A., Beckman, W.A., 2013. Solar Engineering of Thermal Processes. John Wiley & Sons.

Goel, N., Taylor, R.A., Otanicar, T., 2020. A review of nanofluid-based direct absorption solar collectors: Design considerations and experiments with hybrid PV/Thermal and direct steam generation collectors. Renew. Energy 145, 903–913.

Gorji, T.B., Ranjbar, A.A., 2016. A numerical and experimental investigation on the performance of a low-flux direct absorption solar collector (DASC) using graphite, magnetite and silver nanofluids. Sol. Energy 135, 493–505.

Gupta, H.K., Agrawal, G.D., Mathur, J., 2015. An experimental investigation of a low temperature Al2o3-H2O nanofluid based direct absorption solar collector. Sol. Energy 118, 390–396.

He, Q., Yan, G., Wang, S., 2016. Experimental investigation on solar thermal properties of magnetic nanofluids for direct absorption solar collector. In: ASME 2016 5th International Conference on Micro/Nanoscale Heat and Mass Transfer. American Society of Mechanical Engineers Digital Collection.

Hydromx, 2021. Energy saving solution. https://www.hydromx.com/.

Idelchik, I.E., 1986. Handbook of hydraulic resistance. Washington.

Jin, H., Lin, G., Guo, Y., Bai, L., Wen, D., 2020. Nanoparticles enabled pump-free direct absorption solar collectors. Renew. Energy 145, 2337–2344.

Jin, H., Lin, G., Zeiny, A., Bai, L., Cai, J., Wen, D., 2019. Experimental study of transparent oscillating heat pipes filled with solar absorptive nanofluids. Int. J. Heat Mass Transfer 139, 789–801.

Karami, M., Akhavan-Bahabadi, M.A., Delfani, M., 2015. Experimental investigation of CuO nanofluid-based direct absorption solar collector for residential applications. Renew. Sustain. Energy Rev. 52, 793–801.

Kumar, S., Sharma, V., Samantaray, M.R., Chander, N., 2020. Experimental investigation of a direct absorption solar collector using ultra stable gold plasmonic nanofluid under real outdoor conditions. Renew. Energy 12, 1958–1969.

Lassoued, A., Lassoued, M.S., Dkhil, B., Ammar, S., Gadri, A., 2018. Synthesis, photoluminescence and magnetic properties of iron oxide (α-Fe2O3) nanoparticles through precipitation or hydrothermal methods. Physica E 101, 212–219.

Lewis, R.W., Nithiarasu, P., Seetharamu, K.N., 2004. Fundamentals of the Finite Element Method for Heat and Fluid Flow. John Wiley & Sons.

Liu, Z., Yan, Y., Fu, R., Alsaady, M., 2018. Enhancement of solar energy collection with magnetic nanofluids. Therm. Sci. Eng. Progress 8, 130–135.

Moldoveanu, G.M., Huminic, G., Minea, A.A., Huminic, A., 2018. Experimental study on thermal conductivity of stabilized Al2O3 and SiO2 nanofluids and their hybrid. Int. J. Heat Mass Transfer 127, 450–457.

Moravej, M., Doranehgard, M.H., Razeghizadeh, A., Namdarnia, F., Karimi, N., Li, L.K., Mozafari, H., Ebrahimi, Z., 2021. Experimental study of a hemispherical three-dimensional solar collector operating with silver-water nanofluid. Sustain. Energy Technol. Assess. 44, 101043.

Muench, G.J., Arajs, S., Matijević, E., 1981. Magnetic properties of monodispersed submicromic α-Fe2O3 particles. J. Appl. Phys. 52 (3), 2493–2495.

Otanicar, T.P., Phelan, P.E., Prasher, R.S., Rosengarten, G., Taylor, R.A., 2010. Nanofluid-based direct absorption solar collector. J. Renew. Sustain. Energy 2 (3), 033102.

Popsueva, V., Lopez, A.F.O., Kosinska, A., Nikolaev, O., Balakin, B.V., 2021. Field study on the thermal performance of vacuum tube solar collectors in the climate conditions of Western Norway. Energies 14 (10), 2745.

Rudyak, V.Y., Minakov, A.V., 2018. Thermophysical properties of nanofluids. Eur. Phys. J. E 41 (1), 1–12.

Sigma Aldrich, 2021. Iron (III) oxide, nanopowder, <50 nm. https://www.sigmaaldrich.com/NO/en/product/aldrich/544884.

Singh, N., Khullar, V., 2020. On-sun testing of volumetric absorption based concentrating solar collector employing carbon soot nanoparticles laden fluid. Sustain. Energy Technol. Assess. 42, 100868.

Struchalin, P., Yunin, V., Kutsenko, K., Nikolaev, O., Vologzhannikova, A., Shevelyova, M., Gorbacheva, O., Balakin, B., 2021. Performance of a tubular direct absorption solar collector with a carbon-based nanofluid. Int. J. Heat Mass Transfer 179, 121717.

Ulset, E.T., Kosinski, P., Zabednova, Y., Zhdaneev, O.V., Struchalin, P.G., Balakin, B.V., 2018. Photothermal boiling in aqueous nanofluids. Nano Energy 50, 339–346.

Vakili, M., Hosseinalipour, S.M., Delfani, S., Khosrojerdi, S., Karami, M., 2016. Experimental investigation of graphene nanoplatelets nanofluid-based volumetric solar collector for domestic hot water systems. Sol. Energy 131, 119–130.

Viskanta, R., 1987. Direct absorption solar radiation collection systems. In: Solar Energy Utilization. Springer, pp. 334–360.